J Nanopart Res (2012) 14:1025
DOI 10.1007/s11051-012-1025-z

RESEARCH PAPER

Au/SiO_2/QD core/shell/shell nanostructures with plasmonic-enhanced photoluminescence

Ping Yang · Kazunori Kawasaki · Masanori Ando · Norio Murase

Received: 29 November 2011 / Accepted: 29 June 2012 / Published online: 5 August 2012

Abstract A sol–gel method has been developed to fabricate Au/SiO_2/quantum dot (QD) core–shell–shell nanostructures with plasmonic-enhanced photoluminescence (PL). Au nanoparticle (NP) was homogeneously coated with a SiO_2 shell with adjusted thickness through a Stöber synthesis. When the toluene solution of hydrophobic CdSe/ZnS QDs was mixed with partially hydrolyzed 3-aminopropyltrimethoxysilane (APS) sol, the ligands on the QDs were replaced by a thin functional SiO_2 layer because the amino group in partially hydrolyzed APS has strong binding interaction with the QDs. Partially hydrolyzed APS plays an important role as a thin functional layer for the transfers of QDs to water phase and the subsequent connection to aqueous SiO_2-coated Au NPs. Although Au NPs were demonstrated as efficient PL quenchers when the SiO_2 shell on the Au NPs is thin (less than 5 nm), we found that precise control of the spacing between the Au NP core and the QD shell resulted in QDs with an enhancement of 30 % of PL efficiency. The Au/SiO_2/QD core/shell/shell nanostructures also reveal strong surface plasmon scattering, which makes the Au/SiO/QD core–shell–shell nanostructures an excellent dual-modality imaging probe. This technology can serve as a general route for encapsulating a variety of discrete nanomaterials because monodispersed nanostructures often have a similar surface chemistry.

Keywords Quantum dot · Au · Nanoparticle · Plasmon · Photoluminescence · Enhancement · Sol–gel method

Introduction

Fluorescence imaging has been widely used in clinical diagnosis and monitoring processes in biological systems. Regardless of the measurement technique used, the photoluminescence (PL) intensity produced by a fluorescent probe is of crucial importance in determining its capability to provide specific detection of materials of interest in the presence of unknown amounts of other substances (Gisin et al. 2002; Wang et al. 2010). The development of contrast agents, such as fluorescent probes with engineered biomarker functionalities, has become necessary for the advancement of new bioimaging technologies (Hillman and Moore 2007).

Electronic supplementary material The online version of this article (doi:10.1007/s11051-012-1025-z) contains supplementary material, which is available to authorized users.

P. Yang · K. Kawasaki · M. Ando · N. Murase
Health Research Institute, National Institute of Advanced Industrial Science and Technology, Midorigaoka, Ikeda-city, Osaka 563-8577, Japan

N. Murase (✉)
Health Research Institute, National Institute of Advanced Industrial Science and Technology, Hayashi-cho, Takamatsu, Kagawa 761-0395, Japan
e-mail: n-murase@aist.go.jp

The plasmon resonant properties of metallic nanoparticles (NPs) can be controlled by optimizing the NP topology, dimensions, and composition. When plasmonic NPs are smaller than a wavelength of light, they become absorbers, much like molecules. Coupling of excited fluorophores into surface plasmons is well known to occur for intermediate metal–particle separations (Barnes 1998; Noginov et al. 2009). This effect is the basis for surface plasmons-coupled emission, which takes advantage of coupling between excited emitters and surface plasmons to excite surface plasmons that are then scattered into photons and detected (Lackowicz, 2004; Gryczynski et al. 2005)

Metallic NPs have been revealed to enhance the PL and decrease the molecular excited-state lifetimes of vicinal fluorophores. The PL enhancement is attributable to a combination of processes including enhanced absorption by the molecule, modification of the radiactive decay rate of the molecule, and enhanced coupling of the fluorescent emission to the far field (Wang et al. 2010). The extent of the enhancement that can be achieved by coupling of quantum dots (QDs) to metal nanostructures or rough films, strongly depends on the proximity of the QDs to the metal structure, and has been demonstrated to decay exponentially with increasing distance between the two (Chan et al. 2009; Ozel et al. 2011). Experimental studies have demonstrated over 20 times enhancement in emission intensity for emitters coupled to surface plasmon supporting NPs compared with sources placed on glass or other non-plasmon supporting substrates (Okamoto et al. 2006; Pompa et al. 2006; Song et al. 2005). Despite these recent advances achieved on surfaces or based on NPs in films, a long-standing barrier has been how to functionalize QDs with plasmonic materials such as Au NPs. A challenge will be maintaining the unique electronic and optical properties of both nanocomponents and making discrete hybrid structures with tunable separation in the nanometer regime.

CdSe/ZnS QDs have attracted much attention due to their excellent PL properties, including size-dependent narrow emission, large absorption cross section, high PL efficiency at room temperature, and excellent photostability (Gerion et al. 2001). The QDs are typically synthesized in high boiling point, non-polar organic solvents to obtain high quality, monocrystalline particles with narrow size distributions. The QDs are stabilized by hydrophobic ligands (Bruchez et al. 1998). Recently, we found out partially hydrolyzed silane agents have an ability to replace the hydrophobic ligands on the CdSe/ZnS QDs without deteriorating their PL properties (Yang et al. 2010). This could be a unique technique to transfer the QDs into water phase for further applications because such SiO_2 layer can reduce the surface deterioration of the QDs. For the bio-applications of QDs, silica is an ideal matrix because of its good mechanical and optical properties compared with polymers (Murase 2010). There have been many reports describing the deposition of an SiO_2 layer on semiconductor QDs (Selvan et al. 2005; Nann and Mulvaney 2004; Salgueiriño-Maceira et al. 2006; Yang and Murase 2010) and Au NPs (Yi et al. 2006; Liz-Marzán et al. 1996) which exhibited important applications for biosensors. There have been several reports focused on the plasmonic-enhanced luminescence of metal/SiO_2/QD composite nanostructures. For example, Liu and co-workers reported on the hybrid Au/SiO_2/QD superstructures with plasmonic-enhanced PL (Liu et al. 2006). However, the size of the superstructures is $\sim$100 nm. This size is too bulky for the efficient labeling of fine subcellular features. Therefore, novel method is still expected to develop plasmonic-enhanced luminescent nanostructures with small size for supersensitive detection.

In this article, we report on the synthesis of well-defined hybrid nanostructures consisted of Au NP core over coated with a SiO_2 shell, followed by a dense layer of colloidal CdSe/ZnS QDs. The silanization of the QDs enabled them to be transferred from toluene to water. The dielectric SiO_2 layer with tunable thickness provides a simple means for adjusting the interactions between the QDs and the Au NP core. The nanostructures exhibited plasmonic-enhanced PL when the thickness of SiO_2 layer was optimized. Because the QDs in the nanostructure are coated with a functional SiO_2 layer with amino groups, the nanostructures are easily conjugated with biomolecules for further applications.

Experimental section

Chemicals

All chemicals unless specified were obtained from Sigma Aldrich and used as received. Chemicals were

of analytical grade or of the highest purity available. The pure water was obtained from a Milli-Q synthesis system. Hydrophobic CdSe/ZnS QDs were supplied by Evident.

Preparation of Au NPs

Citrate-stabilized Au NPs were synthesized according to the reported method (Yang et al. 2011). Briefly, 90 mg sodium citrate was dissolved in 100 mL H_2O with vigorous stirring and heated to 100 °C. 1 mL of 50 mM $HAuCl_4$ was injected into the solution with a speed of 0.2 mL/min. The reaction mixture was maintained at the boiling temperature for further 3 min before allowing to cool down to room temperature. The initial colloidal solution of Au was condensed by a 3000-MWCO filter at 6,000 rpm (4,800 g) for several times to remove un-reacted materials for the purpose of preventing the NPs from agglomeration.

Preparation of SiO_2 beads with Au NPs

Single Au NP coated with a homogeneous SiO_2 shell was carried out by using a Stöber process. Typically, 1 ml of 1 μM re-dispersed Au colloid was added in the mixture of 8 mL ethanol and 0.1 mL 25 % ammonia with vigorous stirring. The concentration and injection speed of TEOS were precisely adjusted according to the thickness of SiO_2 shell (Yang et al. 2011). The as-prepared SiO_2-coated Au NPs were centrifuged at 15,000 rpm for 10 min and then re-dispersed in H_2O for further characterization.

Preparation of Au/SiO_2/QD core–shell–shell nanostructures

A precursor APS sol was prepared by mixing APS with ethanol and H_2O. Typically, the molar ratio of ethanol/H_2O/APS is 30/1.5/1. The mixture was stirred for 15–24 h and then heat-treated at 50–70 °C to evaporate the ethanol. The toluene solution of CdSe/ZnS QDs (0.1–1 mL) was mixed with the precursor APS sol of 0.2–0.5 mL with stirring for 5–10 min. Colloidal solution of SiO_2-coated Au NPs of 0.1–0.5 mL was added to the mixture with stirring for 10 min. Finally, Au/SiO_2/QD core–shell–shell nanostructure was created accompanied by a phase separation. Toluene was remained on the upper part. The APS sol with the Au/SiO_2/QD nanostructure was extracted and centrifuged at 14,500 rpm for 2 min with several times for purification. For comparison, the phase transfer of the QDs was carried out by using pure water instead of a colloidal solution of SiO_2-coated Au NPs.

Apparatus

Observations by TEM were carried out using mainly a Hitachi EF-1000 electron microscope. Absorption and PL spectra were taken using conventional spectrometers (Hitachi U-4000 and F-4500). The PL efficiency (η) of luminescent materials represents the number of emitted photons per number of absorbed photons (Murase and Li 2008; Grabolle et al. 2009). Briefly, the PL and absorption spectra of the standard quinine solution (quinine in 0.1 N H_2SO_4 solution, PL efficiency η_0 of 55 %) were measured in a quartz cell of 1 cm as a function of its concentration. The emission intensity P_0 (in the unit of the number of photons) is expressed by the efficiency η_0 as:

$$P_0 \approx K\eta_0 a_0 10^{-0.5a_0},$$

where a_0 is absorbance at the excitation wavelength (365 nm), K is the apparatus function. After the measurement of the absorbance a and PL intensity P of the sample using the same apparatus parameters, the PL efficiency η of the sample is derived by comparing with the PL intensity P_0 of the quinine solution. The error in the PL efficiency is estimated to be within 10 % by comparing the results using two standards including quinine and rhodamine 6G. The PL lifetimes were measured using a time-correlated single-photon counting spectrofluorometer system (FluoroCube-3000U, Horiba). The recorded decay curves were fitted with a multiexponential function by a least squares fitting method.

Results and discussion

Hybrid Au/SiO_2/QD nanostructures were synthesized via a multistep procedure including the synthesis of Au NPs, Au NPs coated with a SiO_2 shell, CdSe/ZnS QDs coated with functional SiO_2 layer with $–NH_2$ groups, and finally the assembly of the functional SiO_2-coated QDs onto the surface of SiO_2-coated Au NPs as illustrated in Scheme 1. The details for the preparation

were explained in "Experimental" section. The result of each step was monitored by measuring the evolution of the properties of the QDs during the formation of the nanostructures as explained below.

Properties of Au NPs

Au NPs with a mean size of 11.4 nm in diameter were prepared according to the standard sodium citrate reduction method. Figure 1 shows the absorption spectrum and the transmission electron microscopy (TEM) image of as-prepared Au NPs. The absorption spectrum of the Au NPs shows the NPs with a very intense surface plasmon absorption band in the visible range (around 520 nm). The exact position of this plasmon band is extremely sensitive to particle size, shape, and the optical and electronic properties of the medium surrounding the particles. Purification process was used to avoid the self-assembly of Au NPs during separation as explained in "Experimental" section. The TEM image indicates the Au NPs were monodispersed in water.

Coating of Au NPs with SiO_2 shell

Colloidal Au NPs is usually composed of single-crystalline, singly twinned, or multiply twinned structures. These nonideal spherical NPs have different crystalline facets with different chemical activities. This makes the chemical affinity of Au surface low to SiO_2. Therefore, amino-terminated silane coupling agents or polymers are often used as the

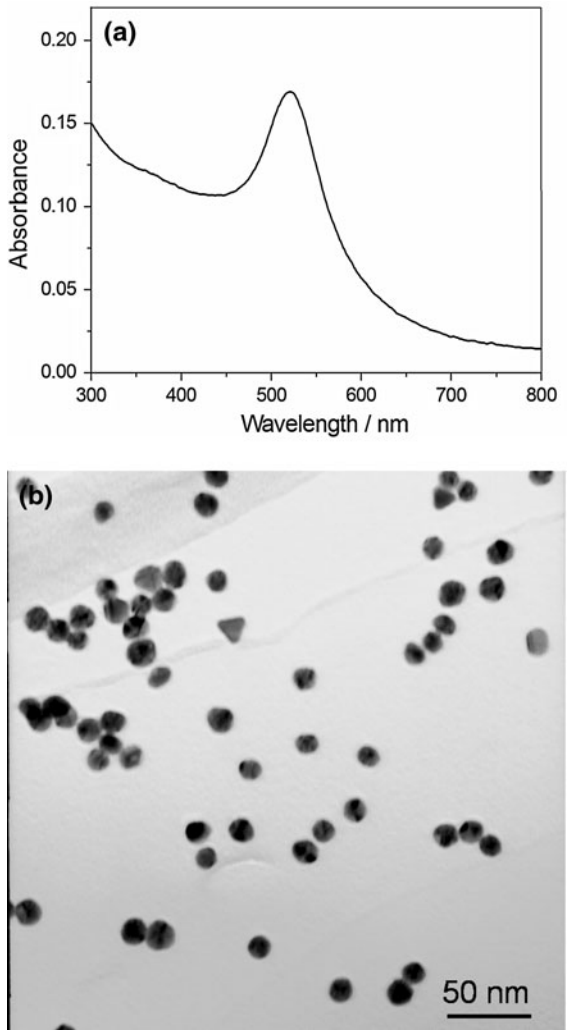

Fig. 1 Absorption spectrum (**a**) and TEM image (**b**) of Au NPs

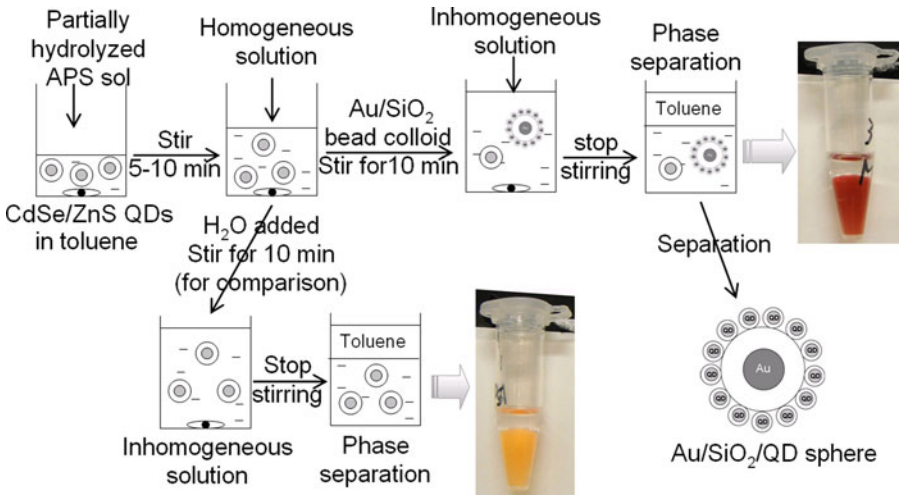

Scheme 1 Preparation procedure of Au/SiO_2/QD nanostructures. Similar phase transfer of CdSe/ZnS QDs was observed by using pure H_2O instead of the aqueous solution of Au/SiO_2 beads

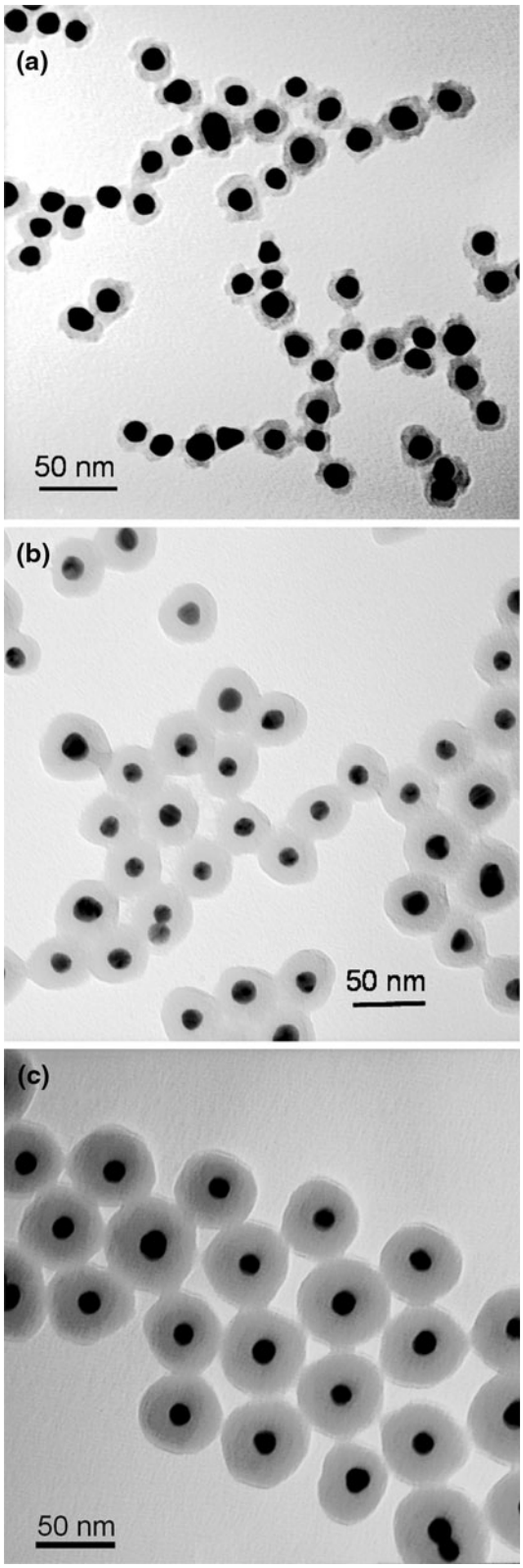

◄ **Fig. 2** TEM images of Au NPs coated with SiO_2 shell with tunable thickness: **a** Bead 1; **b** Bead 2; **c** Bead 3. The mean thickness of SiO_2 shell for Beads 1–3 is 5, 12.5, and 20 nm, respectively

primer to make the Au surface vitreophilic for subsequent SiO_2 coating. Mulvaney and co-workers first reported a three–step procedure for coating Au NPs with a SiO_2 shell using a silane coupling agent as the surface primer (Liz-Marzán et al. 1996). As for directly coated Au NPs with a SiO_2 shell without a primer, the controlling of sol–gel procedure is necessary. We found out the slow deposition rate of SiO_2 monomers makes Au NPs coated with a homogeneous SiO_2 shell as explained below.

Figure 2 shows the TEM image of Au NPs encapsulated in SiO_2 beads: (a), Bead 1; (b), Bead 2; (c), Bead 3. The amount of TEOS used for Beads 1–3 was 3, 5, and 9 μL, respectively. The injection speed of TEOS is 0.2 μL/min. In Fig. 2a, inhomogeneous SiO_2 coating was clearly observed. With increasing the amount of TEOS from Beads 1–3, inhomogeneous parts were filled out and become homogeneous. This phenomenon is related to a prior deposition of SiO_2 monomers to a certain facet (Murase 2010). The thickness of SiO_2 shell was easily adjusted by changing the amount of TEOS. For Beads 2 and 3, Au NPs were coated homogeneously with a SiO_2 shell.

We also characterized the absorption spectra of Au/SiO_2 beads. SiO_2 is electronically inert (it does not exchange charge with the Au NPs), but its refractive index is different from that of both water and ethanol (and of course from that of Au). The plasmon absorption band becomes intense with increasing the thickness of SiO_2 shell as shown in Fig. 3. This is due to the increase in the local refractive index around the Au NPs. When the SiO_2 shell becomes sufficiently thick, scattering becomes significant, resulting in a strong increase in the apparent absorbance at shorter wavelengths. Compared with that of Au NPs, the absorption peak wavelength of Au/SiO_2 bead revealed a small red shift as shown in Fig. 3.

Surface silanization by (3-aminopropyl)-trimethoxysilane (APS) and phase transfer of CdSe/ZnS QDs

Phase transfer is an important step for fabricating Au/SiO_2/QD nanostructures. We investigated the

phase transfer of hydrophobic CdSe/ZnS QDs by coating with a functional SiO_2 layer by using partially hydrolyzed APS sol. CdSe/ZnS QDs with hexadecylamine (HDA) as capping agent were transferred into water from toluene by silanization as demonstrated in Scheme 1. When the toluene solution of the QDs was mixed with partially hydrolyzed APS sol, a transparent mixture was obtained because the partial hydrolysis made APS molecules amphiphilic. The amino group in partially hydrolyzed APS attached to the QDs instead of organic ammine because of strong binding interactions between the QDs and the $–NH_2$ ligands in APS. The phase transfer of the QDs occurred when pure water was added in the mixture since partially hydrolyzed APS on the QD surface is hydrophilic. This QD phase transfer technique is simple and sufficiently efficient because all the QDs were transferred into water phase within several minutes. Finally, the QDs with functional SiO_2 layer were separated for further characterization. Partially hydrolyzed APS sol thus prepared is a key to transfer the QDs into water and to avoid the agglomeration of the QDs during phase transfer. Additional experimental results indicated CdSe/ZnS QDs aggregated when pure APS (little amount), water, and ethanol were added in the toluene solution of the QDs.

Formation and properties of $Au/SiO_2/QD$ core–shell–shell nanostructures

The formation mechanism of the $Au/SiO_2/QD$ core–shell–shell nanostructure is demonstrated in Scheme 2. In this process, partially hydrolyzed APS plays an important role to create the nanostructures. Partially hydrolyzed APS molecules act as linkers between SiO_2-coated Au NPs and CdSe/ZnS QDs.

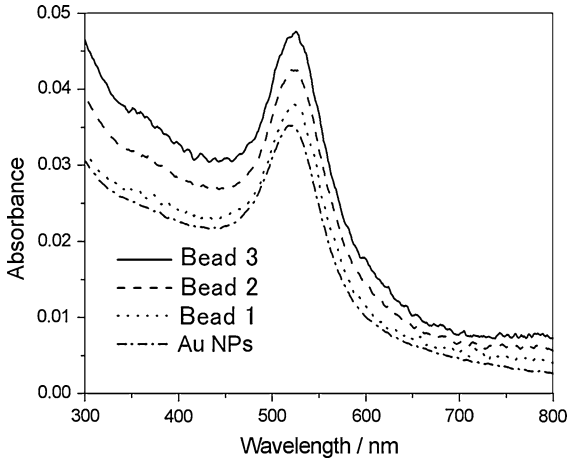

Fig. 3 Absorbance spectra of Au NPs and SiO_2-coated Au NP

The functional SiO_2-coated QDs prepared above were transferred into the aqueous solution of SiO_2-coated Au NPs since partially hydrolyzed APS is hydrophilic. Due to the electrostatic interactions between the functional SiO_2-coated QDs and SiO_2 shell on Au NPs, the QDs self-assembled onto the surface of the SiO_2 shell, resulting in the formation of hybrid $Au/SiO_2/QD$ superstructures.

Figure 4 shows the TEM image of $Au/SiO_2/QD$ nanostructure prepared by using Bead 2 shown in Fig. 2. The detailed 3D images are shown in Fig. S1 (Supporting information). The result clearly indicates the nanostructure with a Au NP core, SiO_2 shell and the QDs layer. In this example, the Au NP core has a mean diameter of 11.4 nm. The thickness of SiO_2 shell is $\sim$12. 5 nm. The $Au/SiO_2/QD$ nanostructures with a diameter of less than 50 nm are spherical and highly monodispersible. CdSe/ZnS QDs form dense monolayer on all of the SiO_2-coated

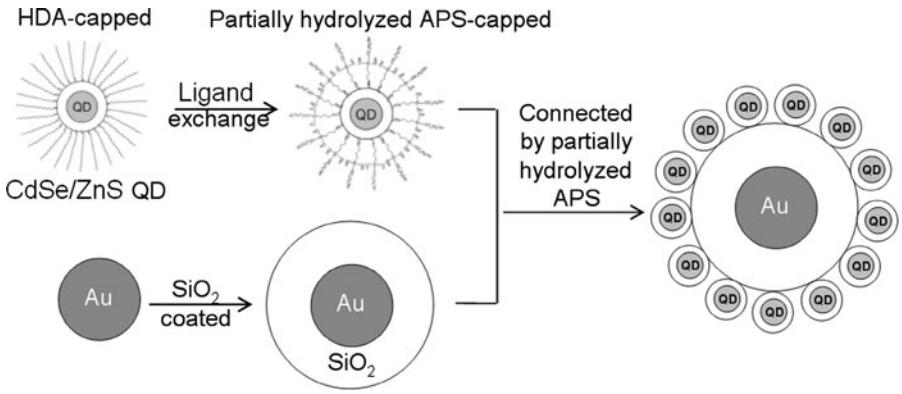

Scheme 2 Formation procedure of $Au/SiO_2/QD$ nanostructure

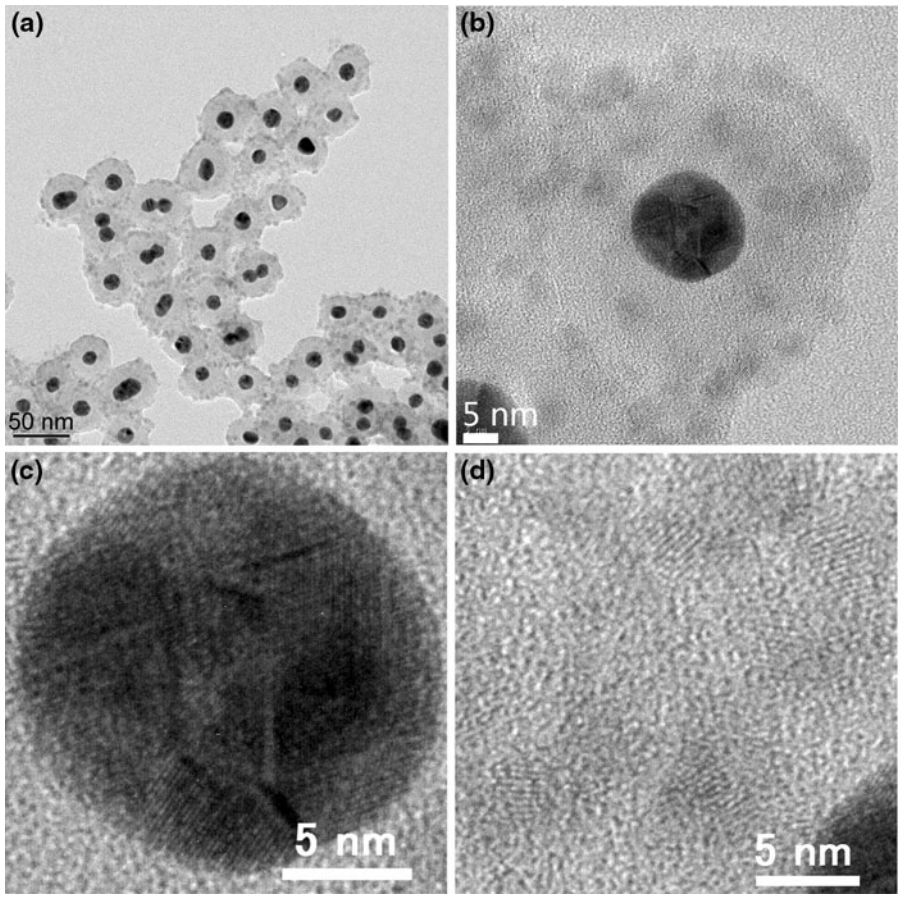

Fig. 4 TEM images of Au/SiO_2/QD nanostructure prepared by Bead 2 shown in Fig. 2 (same specimen at different magnification). The mean size of the nanostructure was ~ 47 nm in diameter (**a**, **b**). The images show the QDs were attached on the nanostructures. The images with high magnification show clearly the lattice fringes of Au NP (**c**) and QDs (**d**)

Au NPs. This indicates the strong binding force between SiO_2-coated Au NPs and functional SiO_2-coated QDs is a key for the formation of the nanostructures. Because of APS gel on the surface, Au/SiO_2/QD nanostructures easily aggregated in water as shown in Fig. 4. Such APS gel also resulted in an optical scattering observed in absorption spectra as shown in Fig. 5.

To evaluate the effect of the thickness of SiO_2 shell on the PL properties of the Au/SiO_2/QD nanostructures, three kinds of SiO_2-coated Au NPs (Beads 1–3 shown in Fig. 2) were used to fabricate the nanostructure. Figure 5 shows the absorption and PL spectra of these nanostructures. The absorption and PL spectra of functional SiO_2-coated QDs are shown for comparison. To eliminate the effect of scattering on the calculation of PL efficiency, the concentration of QDs and scattering generated by beads and APS gel in the solution of functional SiO_2-coated QDs were adjusted. For example, Bead 2 and functional SiO_2-coated QDs thus prepared exhibited the same absorption component in every wavelength as shown in Fig. 5b. An increased PL efficiency of 30 % was clearly observed from the nanostructure prepared by Bead 2 compared with functional SiO_2-coated QDs. When the thickness of SiO_2 shell is 20 nm (using Bead 3), the PL efficiency of the nanostructure is very similar to that of functional SiO_2–coated QDs. However, the PL efficiency of the nanostructure prepared by Bead 1 with a SiO_2 shell of 5 nm revealed a decrease of 40 % compared with functional SiO_2-coated QDs. The absorption spectrum of the nanostructures shows an intense surface plasmon absorption band in the visible range (around 520 nm for Beads 1–3). This excellent

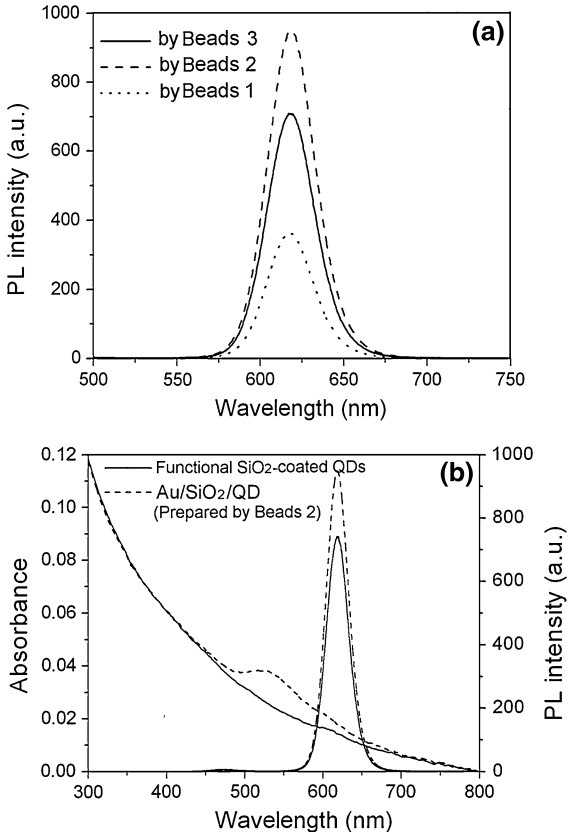

Fig. 5 Absorption and PL spectra of partially hydrolyzed functional SiO_2-coated QDs and Au/SiO_2/QD composite nanostructure: **a** PL spectra of Au/SiO_2/QD nanostructures prepared by Beads 1–3 shown in Fig. 2 (excited at 365 nm, QD concentrations are same for these three samples); **b** absorption and PL spectra of functional SiO_2-coated QDs and Au/SiO_2/QD nanostructure prepared by Bead 2. PL efficiency of 28 % enhancement was observed from the nanostructure prepared by Bead 2 compared with functional SiO_2-coated QDs. The absorbance of the nanostructure at 800 nm was set to zero for comparison

dual-property indicates the nanostructure is well applicable for imaging probes.

It is well known that the presence of a metal surface in close proximity to a fluorophore can significantly modify its emission. This has been attributed to several factors, and depends strongly on the distance between fluorophore and metal (Lackowicz 2001; Barnes 1998). For the Au/SiO_2/QD nanostructures prepared by Bead 3, no affect on the PL efficiency was observed. This is ascribed that PL is not affected by Au NPs and behaves as they would be in free space. As separation distance decreases, increased non-radiative relaxation of the excited fluorophore occurs as energy is coupled

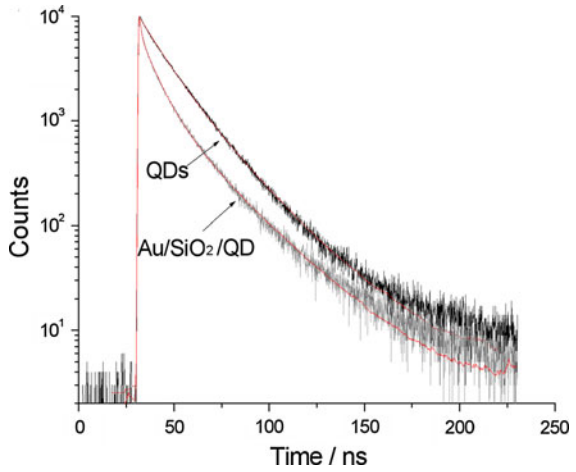

Fig. 6 PL decay curves (measured at maximum emission peak, $\lambda_{ex} = 374$ nm) of CdSe/ZnS QDs in toluene solution and in Au/SiO_2/QD nanostructure in H_2O. Reproduced curves using the data illustrated in Table 1 are plotted as *thin red lines*

Table 1 Components B_1 and B_2, time constants τ_1 and τ_2, and average lifetime τ of CdSe/ZnS QDs and Au/SiO_2/QD core–shell–shell nanostructures prepared by Bead 2

Samples	B_1 (%)	B_2 (%)	τ_1/ns	τ_2/ns	τ/ns	PL efficiency (%)
QDs	44.1	55.9	10.7	22.8	19.5	18
Au/SiO_2/QD	34.2	65.8	4.8	20.8	19.1	23

into surface plasmons on the surface of the metal. Therefore, an increased PL efficiency was observed for the nanostructure prepared by Bead 2. For very small separations, such as the ones prepared by Beads 1, emission quenching occurs and is attributed to damping of dipole oscillators and coupling of energy into evanescent waves at the surface of the metal. Figure 6 shows the PL decay profiles of the initial CdSe/ZnS QDs and the QDs coupled to SiO_2-coated Au NPs prepared by Bead 2 shown in Fig. 2. The decay curves can be well fitted to a biexponential model described by $F(t) = A + B_1\exp(-t/\tau_1) + B_2\exp(-t/\tau_2)$, where τ_1 and τ_2 ($\tau_1 < \tau_2$) represent the time constants, and B_1 and B_2 represent the amplitudes of the fast and slow components, respectively. Average lifetime τ is calculated using $\tau = (B_1\tau_1^2 + B_2\tau_2^2)/(B_1\tau_1 + B_2\tau_2)$ (Jones et al. 2003). The fitted values of the parameters B_1, B_2, τ_1, τ_2, and average lifetime τ are listed in Table 1.

For initial CdSe/ZnS QDs in a toluene solution, the decay profile reveals an average lifetime of 19.5 ns. The PL lifetime of the QDs is extremely sensitive to the size of CdSe core, the thickness of ZnS shell, and surface ligands. The fast (τ_1), and slow (τ_2) decay of CdSe/ZnS QDs involves recombination of the delocalized carriers and the localized carriers, respectively. The fast component (B_1) of PL decay of the QDs in the Au/SiO_2/QD nanostructures decreased compared with that of initial QDs, while the slow component (B_2) increased. As illustrated in Table 1, the lifetime of fast PL decay (τ_1) drastically decreased; however, the lifetime of slow PL decay (τ_2) decreased slightly, which is characteristic for the localization process of excitons (Rogach et al. 2000). The average lifetime (19. 1 ns) of the nanostructures just revealed a slight decrease compared with the initial QDs. Similar phenomenon was observed in literature. For example, Ozel et al. (2011) observed a significant shortening of PL decay lifetimes for each set of Au NP and CdTe QD films. The photon decay lifetime of CdTe QDs is modified from 7.9 to 1.8 ns in the presence of metal NPs and to 2.8 ns in the presence of metal NPs separated with dielectric layers, which corresponds to the strongest emission enhancement. Yuan and co–worker coupled CdSe/ZnS QDs to Ag nanoprisms using a polymer layer with optimized thickness of 10 nm to minimize energy transfer from QDs to Ag nanoprisms (Yuan et al. 2009). For reference QDs, the decay is single-exponential with an average lifetime of $\sim$25 ns. In contrast, the PL decay profile for coupled QDs deviates slightly from a single-exponential decay with a shortened averaged lifetime of $\sim$5 ns. This phenomenon indicated the lifetime of metal/QDs nanocomposite is sensitive to the structure.

Metallic NPs influence the PL efficiency and lifetime of adjacent fluorophores in a manner dependent on the properties of the nanostructure. There are two kinds of interaction mechanisms between QDs and metal nanostructures (Liu et al. 2006). One mechanism is the modification of the electric field near the metal surface, which changes both the field applied to the QD and the field radiated by it. Another effect is damping induced by energy transfer from the emitter to the metal, which can be described in terms of Joule heating. Because of the competition between field enhancement and non-radiative damping due to energy transfer to surface plasmons, the proximal metal can either enhance or decrease the PL intensity. Damping induced by the metal is strongly distance-dependent (Gersten and Nitzan 1981). In addition, the enhancement and decrease of PL intensity depend strongly on the composition and structure of QDs, metal NPs and intermaterials. PL and time-resolved fluorescence characteristics support each other. Here their modified PL spectra can be explained by a dominating increase in the non-radiative decay rate in the presence of metal NPs (with no dielectric spacer), which results in quenched fluorescence, and by a dominating increase in the radiative decay rate in the presence of metal NPs separated by dielectric layers, which results in enhanced PL, with the combination of enhanced local electric fields in the close proximity of plasmon-coupled QDs (Ozel et al. 2011).

In our experiments, we monitor the change in the PL intensity induced by the competing processes of field enhancement and non-radiative damping which can simultaneously quench and enhance the QD PL depending on the spacing between the two materials and the spectral overlap between the QD PL and the Au surface plasmon resonance (SPR). At short separation distance and significant overlap between QD emission and Au SPR bands, the quenching effect dominates, whereas moderate separation distance and spectral overlap of QD emission and Au SPR result in more pronounced field enhancement. In our Au/SiO_2/QD nanostructures, the enhanced PL efficiency was observed under the optimal SiO_2 shell thickness of $\sim$12.5 nm. Similarly, using Au NP films on a glass surface, the QD PL could be enhanced by adjusting the QD and Au NP separation with polyelectrolytes (Kulakovich et al. 2002).

Conclusions

We have developed a multistep synthesis of hybrid nanostructures consisted of Au NP core, dielectric SiO_2 layer, and dense layers of CdSe/ZnS QDs. The QDs on the nanostructures were coated with a functional SiO_2 layer with amino groups on the surface. The nanostructures with a mean size of less than 50 nm also exhibited an intense surface plasmon absorption band. This architecture allows for versatile control of QD–Au NP interactions through control of the thickness of the dielectric spacer. With such configuration, we achieved 1.3 times enhancement of the PL efficiency and a slight decrease of PL lifetime

accompanied by the decrease of fast component and the increase of slow component. The PL enhancement depended strongly on the thickness of dielectric SiO_2 layer. The observed characteristics would make the proposed material a better alternative for a high performance single-photon emitter.

References

Barnes WL (1998) Fluorescence near interfaces: the role of photonic mode density. J Mod Opt 45:661–699. doi:10.1080/09500349808230614

Bruchez MP, Moronne M, Gin P, Weiss S, Alivisatos AP (1998) Semiconductor nanocrystals as fluorescent biological labels. Science 281:2013–2016. doi:10.1126/science.281.5385.2013

Chan YH, Chen J, Wark SE, Skiles SL, Son DH, Batteas JD (2009) Using patterned arrays of metal nanoparticles to probe plasmon enhanced luminescence of CdSe quantum dots. ACS Nano 3:1735–1744. doi:10.1021/nn900317n

Gerion D, Pinaud F, Shara Williams SC, Parak WJ, Zanchet D, Weiss S, Paul Alivisatos A (2001) Synthesis and properties of biocompatible water-soluble silica-coated CdSe/ZnS semiconductor quantum dots. J Phys Chem B 105:8861–8871. doi:10.1021/jp0105488

Gersten J, Nitzan A (1981) Spectroscopic properties of molecules interacting with small dielectric particles. J Chem Phys 75:1139–1152. doi:10.1063/1.442161

Gisin N, Ribordy G, Tittel W, Zbinden H (2002) Quantum cryptography. Rev Mod Phys 74:145–195. doi:10.1103/RevModPhys.74.145

Grabolle M, Spieles M, Lesnyak V, Gaponik N, Eychmüller A, Resch–Genger U (2009) Determination of the fluorescence quantum yield of quantum dots: suitable procedures and achievable uncertainties. Anal Chem 81:6285–6294. doi:10.1021/ac900308v

Gryczynski I, Malicka J, Jiang W, Fischer H, Chan WCW, Gryczynski Z, Grudzinski W, Lakowicz JR (2005) Surface-plasmon-coupled emission of quantum dots. J Phys Chem B 109:1088–1093. doi:10.1021/jp046173i

Hillman EMC, Moore A (2007) All-optical anatomical co-registration for molecular imaging of small animals using dynamic contrast. Nat Photonics 1:526–530. doi:10.1038/nphoton.2007.146

Jones M, Nedeljkovic J, Ellingson RJ, Nozik AJ, Rumbles GJ (2003) Photoenhancement of luminescence in colloidal CdSe quantum dot solutions. Phys Chem B 107:11346–11352. doi:10.1021/jp035598m

Kulakovich O, Strekal N, Yaroshevich A, Maskevich S, Gaponenko S, Nabiev I, Woggon U, Artemyev M (2002) Enhanced luminescence of CdSe quantum dots on gold colloids. Nano Lett 2:1449–1452. doi:10.1021/nl025819k

Lackowicz JR (2001) Radiative decay engineering: biophysical and biomedical applications. Anal Biochem 298:1–24. doi:10.1006/abio.2001.5377

Lackowicz JR (2004) Radiative decay engineering 3. Surface plasmon-coupled directional emission. Anal Biochem 324:153–169. doi:10.1016/j.ab.2003.09.039

Liu N, Prall BS, Klimov VI (2006) Hybrid gold/silica/nanocrystal-quantum-dot superstructures: synthesis and analysis of semiconductor-metal interactions. J Am Chem Soc 128:15362–15363. doi:10.1021/ja0660296

Liz-Marzán LM, Giersig M, Mulvaney P (1996) Synthesis of nanosized gold-silica core–shell particles. Langmuir 12:4329–4335

Murase N (2010) Quantum dot–core silica glass–shell nanomaterials: synthesis, characterization, and potential biomedical applications, vol 6. In Kumar C (ed) Nanomaterials for the life sciences. Wiley, New York, p. 393. doi:10.1002/9783527610419.ntls0201

Murase N, Li C (2008) Consistent determination of photoluminescence quantum efficiency for phosphors in the form of solution, plate, thin film, and powder. J Lumin 128:1896–1903. doi:10.1016/j.jlumin.2008.05.016

Nann T, Mulvaney P (2004) Single quantum dots in spherical silica particles. Angew Chem Int Ed 43:5393–5396. doi:10.1002/anie.200460752

Noginov MA, Zhu G, Belgrave AM, Bakker R, Shalaev VM, Narimanov EE, Stout S, Herz E, Suteewong T, Wiesner U (2009) Atmospheric carbon dioxide through the eocene–oligocene climate transition. Nature 460:1110–1114. doi:10.1038/nature08447

Okamoto K, Vyawahare S, Scherer A (2006) Surface-plasmon enhanced bright emission from CdSe quantum-dot nanocrystals. J Opt Soc Am B 23:1674–1678. doi:0740-3224/06/081674-5/

Ozel T, Nizamoglu S, Sefunc MA, Samarskaya O, Ozel IO, Mutlugun E, Lesnyak V, Gaponik N, Eychmuller A, Gaponenko SV, Demir HV (2011) Anisotropic emission from multilayered plasmon resonator nanocomposites of isotropic semiconductor quantum dots. ACS Nano 5:1328–1334. doi:10.1021/nn1030324

Pompa PP, Martiradonna L, Torre AD, Sala FD, Manna L, Vittorio MD, Calabi F, Cingolani R, Rinaldi R (2006) Metal-enhanced fluorescence of colloidal nanocrystals with nanoscale control. Nat Nanotechnol 1:126–130. doi:10.1038/nnano.2006.93

Rogach AL, Nagesha D, Ostrander JW, Giersig M, Kotov NA (2000) "Raisin bun"-type composite spheres of silica and semiconductor nanocrystals. Chem Mater 12:2676–2685. doi:10.1021/cm000244i

Salgueiriño-Maceira V, Correa-Duarte MA, Spasova M, Liz-Marzán LM, Farle M (2006) Composite silica spheres with magnetic and luminescent functionalities. Adv Funct Mater 16:509–514. doi:10.1002/adfm.200500565

Selvan ST, Tan TT, Ying JY (2005) Robust, non-cytotoxic, silica-coated CdSe quantum dots with efficient photoluminescence. Adv Mater 17:1620–1625. doi:10.1002/adma.200401960

Song JH, Atay T, Shi S, Urabe H, Nurmikko AV (2005) Large enhancement of fluorescence efficiency from CdSe/ZnS quantum dots induced by resonant coupling to spatially controlled surface plasmons. Nano Lett 5:1557–1561. doi:10.1021/nl050813r

Wang EH, Smolyaninov II, Davis CC (2010) Surface plasmon polariton enhanced fluorescence from quantum dots on nanostructured metal surfaces. Nano Lett 10:813–820. doi:10.1021/nl9031692

Yang P, Murase N (2010) Size-tunable highly luminescent SiO_2 particles impregnated with number-adjusted CdTe

nanocrystals. ChemPhysChem 11:815–821. doi:10.1002/cphc.200900850

Yang P, Murase N, Suzuki M, Hosokawa C, Kawasaki K, Kato T, Taguchi T (2010) Bright, non-blinking, and less-cytotoxic SiO_2 beads with multiple CdSe/ZnS nanocrystals. Chem Commun 46:4595–4597. doi:10.1039/C002243H

Yang P, Ando M, Murase N (2011) Various Au nanoparticle organizations fabricated through SiO_2 monomer induced self-assembly. Langmuir 27:895–901. doi:10.1021/la103143j

Yi DK, Lee SS, Ying JY (2006) Synthesis and applications of magnetic nanocomposite catalysts. Chem Mater 18:2459–2461. doi:10.1021/cm052885p

Yuan CT, Yu P, Ko HC, Huang J, Tang J (2009) Antibunching single-photon emission and blinking suppression of CdSe/ZnS quantum dots. ACS Nano 3:3051–3056. doi:10.1021/nn900760u